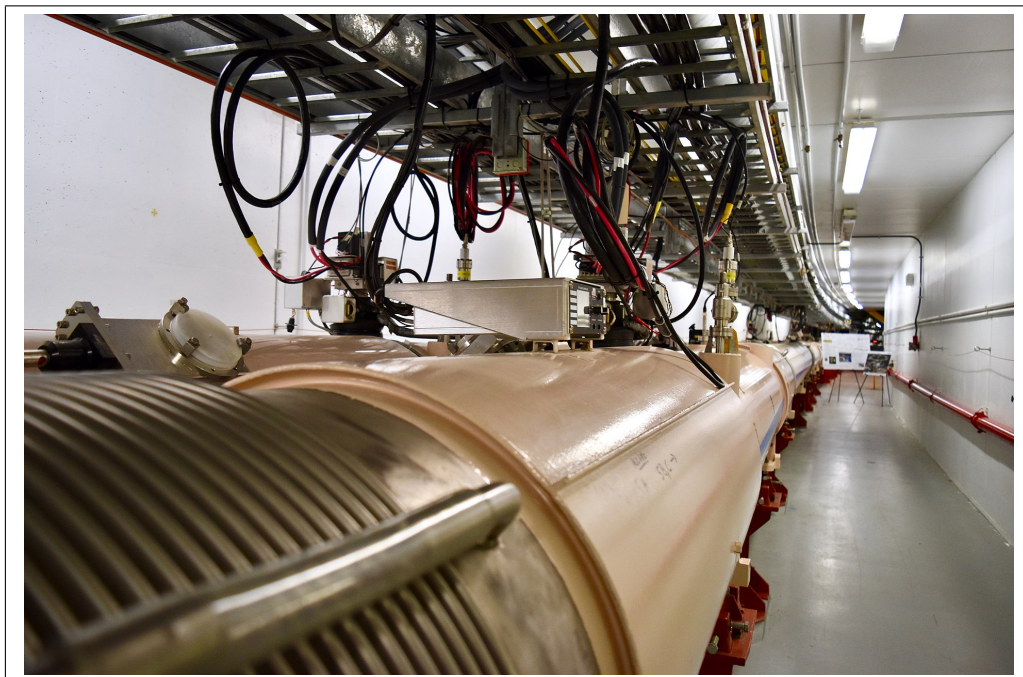**Universiteit Utrecht**

Opleiding Natuur- en Sterrenkunde

A comparison of Au-Au and Pb-Pb quenched jets, using PYTHIA and JEWEL simulations.

BACHELOR THESIS

Rens Meeuwsen

Supervisors:

Dr. Marta VERWEIJ
Universiteit Utrecht

February 27, 2020

Abstract

Comparing JEWEL simulations to PYTHIA simulation shows significantly lower jet width, Soft Drop groomed jet mass and ungroomed jet mass, while a higher $p_T D$ is found. This is observed for comparing 200 GeV p-p PYTHIA to 200 GeV Au-Au JEWEL simulations, as wel as for comparing 5020 GeV p-p PYTHIA to 5020 Pb-Pb JEWEL simulations. Of these shifts in averages the shift in jet width at 200 GeV is largest.

Contents

1   Introduction

Quark-gluon plasma is theorized to be everyhing that was contained in the universe, just microseconds after the Big Bang. Many times denser and hotter than even the interior of our sun, this quark-gluon plasma still holds many mysteries leading experimental physicists are trying to uncover. To reveal the properties this matter gave the universe as it was 14 billion years ago, scientists are colliding heavy ions, such as gold (Au) and lead (Pb) at high energies, to create a quark-gluon plasma. By studying properties of the particles that move through the quark-gluon plasma, created just after the collision, much can be learned about the quark gluon plasma itself.

Enormous particle accelerators are needed for the experiments to create a quark-gluon plasma. Only two accelerators in the world are large enough to reach the energies needed. The first of these two is the Realistic Heavy Ion Collider (RHIC) at the Brookhaven National Laboratory.[2] With this collider the leading research for Au-Au collisions is done.[3] This collider has four detectors, STAR, PHENIX, PHOBOS and BRAHMS. While all detectors are used to study Quark-Gluon Plasma, the STAR detector is most suitable for jet studies. Experiments at RHIC are done at center-of-mass energies of up to $\sqrt{s_{NN}} = 200$ GeV[4].

If we shift our attention from Au-Au collisions to Pb-Pb collisions, we arrive at the second of the two accelerators, the Large Hadron Collider (LHC) at CERN. The largest of the two colliders, the LHC allows for collision at higher center-of-mass energies of up to $\sqrt{s_{NN}} = 5500$ GeV[4]. These heavy ion experiments are mainly done at the ALICE detector, in collaboration with Utrecht University, among others. The other three detectors (ATLAS, CMS and LHCb) are mostly reserved for proton-proton collisions.[5] These proton-proton collisions also take up most of the running time of the LHC, leaving the Pb-Pb experiments just one month a year.

The interactions between the particles created from the collisions will result in more and more particles branching off creating a particle shower, and eventually ending as a collimated beam of hadrons, or jet. These jets are what we will be studying in this thesis. The properties and substructures of these jets will provide information about the constituents of the jets, and this in turn will lead to information about the quark-gluon plasma and the effects this quark-gluon plasma has on the particles interacting with it and moving through it.

We will be studying jet simulations at both 200 GeV and 5020 GeV, comparing jets moving through quark-gluon plasma, or quenched jets, with jets that do not move through quark-gluon plasma, unquenched jets. By comparing the jets at 200 GeV to the jets at 5020 GeV we aim to show, that the quenching has larger observable effects on the jet mass, jet width, $p_T D$ as well as the Soft Drop groomed jet mass at the lower energy of 200 GeV. We will show that among these observables the jet width at 200 GeV is most impacted by jet quenching.

2   Background Theory

2.1   Jets

When particles are collided at RHIC and LHC, what essentially happens is that a large amount of momentum is transferred between the elementary constituents of these particles. Such collision results in a shower of quarks and gluons, a parton shower, with new partons branching off at small angles. This branching of partons continues untill a sufficiently low virtuality is reached for the partons to form hadrons, or *hadronize*. These hadrons are what the calorimeters and trackers in the detectors at RHIC and LHC measure.

The observable jet is the collection of hadrons formed from the partons created in the collision.[6] By studying these jets, we can trace back to the start of these jets and learn about these high-energy partons. While conceptually quite simple, experimentally these jets are far from well-defined. We need some way to say where one jet ends and where the other begins, whether we are looking at one big jet or two smaller ones. To remove as much arbitrariness from this process as possible, a predetermined set of steps to determine the jets is used, a *jet algorithm*. This *jet algorithm* reconstructs the jets, using the final collection of hadrons.

Arguably the most important property used to determine the jet construction is the momentum in the transverse plane p_T. A high p_T indicates a hard QCD process in contrast to the low p_T soft processes. As we take the particle beam in the z-direction, we calculate the transverse momentum p_T as:[6]

$$p_T = \sqrt{p_x^2 + p_y^2}. \tag{1}$$

The *rapidity* y is defined as:[6]

$$y = \frac{1}{2} log \left(\frac{E + p_z}{E - p_z} \right). \tag{2}$$

The jet algorithm mainly used in the fastjet software is the anti-k_t algorithm, though the Cambridge/Aachen algorithm is also used[7]. Both algorithms are a variant of the generalised k_t-algorithm, which works as follows. This algorithm makes a list from the particles in the event, and calculates the *inter-particle distance* and the *beam distance* of these particles.[6] The *inter-particle distance* is calculated as:

$$d_{ij} = min\left(p_{T,i}^{2p}, p_{T,j}^{2p} \right) \Delta R_{ij}^2, \tag{3}$$

with the distance between two particles in the η-ϕ-plane defined as the *beam radius* ΔR:

$$\Delta R^i = \sqrt{(\Delta\phi_i)^2 + (\Delta\eta_i)^2} \tag{4}$$

and p dependent on the type of algorithm. Indices i and j are used to keep track of the particles in the list. The *beam distance* is calculated as:

$$d_{iB} = p_{T,i}^{2p} R^2. \tag{5}$$

The distances d_{ij} and d_{iB} are then iterated over, combining the smallest d_{ij} into a new object k and renaming the smallest d_{iB} jets. For the anti-k_t algorithm, $p = -1$ is used and for the Cambridge/Aachen algorithm $p = 0$ is used.[6]

2.1.1 Jet Observables

With the jets now defined, we can take a look at the substructure of these jets. Let us define the different internal properties of the jets, or *jet observables*. The jet mass M is closely related to the virtuality of the parton that initiated the jet and is defined as:[8]

$$M^2 = \left(\sum_i E_i\right)^2 - \left(\sum_i \vec{p}_i\right)^2, \tag{6}$$

where we sum over the constituents i over the jet. We define the *jet width* W as:[8]

$$W = \frac{\sum_i \Delta R^i p_T^i}{\sum_i p_T^i}, \tag{7}$$

with the *beam radius* ΔR as in equation 4. An observable used to discriminate between gluons and quarks is the jet fragmentation distribution $p_T D$ where the D stand for dispersion:

$$p_T D = \frac{\sqrt{\sum_i p_{T,i}^2}}{\sum_i p_{T,i}}. \tag{8}$$

This variable takes a value between zero and one, with a higher value pointing to quark-jets, while a lower value points to jets containing more gluons.[9]

2.1.2 Jet Grooming

Once a jet has been identified, we can then give different priorities to the different parts of the jet. This process is called *jet grooming*. The jet grooming process we used is called 'Soft Drop'.[10][11] This process uses the anti-k_t algorithm to identify the constituents of the jets and then recluster them using the Cambridge-Aachen algorithm. The Cambridge-Aachen algorithm is especially good at finding the different subjets and after two subjets have been identified the 'Soft Drop' checks whether both jets have a sufficiently high enough p_T or, in other words, are hard. This is done by checking the 'Soft Drop condition':

$$\frac{min(p_{T,1}, p_{T,2})}{p_{T,1} + p_{T,2}} > z_{cut} \left(\frac{\Delta R}{R}\right)^\beta, \tag{9}$$

with z_{cut} and β Soft Drop specific parameters and with indices referring to the two identified subjets. For our simulations $z_{cut} = 0.1$ and $\beta = 0$ were used. This process is repeated until two hard subjets are identified or we have an untagged jet, which cannot be separated into two hard subjets. The momentum fraction z_g between these two subjets is defined as:

$$z_g = \frac{min(p_{T,1}, p_{T,2})}{p_{T,1} + p_{T,2}} \tag{10}$$

This process can then be repeated on both subjets, untill all resulting subjets are untagged.[12]

2.2   Jet Quenching

When the first heavy ion collision experiments were being done at CERN's Super Proton Synchrotron (SPS) and RHIC, they were noticing that some jets were losing energy. This effect has been replicated after these first observations, with one such replication shown in Figure 1 from the ATLAS group at CERN. This energy loss was due to the jets moving through a medium, which is called the quark-gluon plasma. This process of jets losing energy, when moving through the quark-gluon plasma, we call *jet quenching*. This quark-gluon plasma is extremely hot and dense, much akin to the state of the universe just after the Big Bang. Thus by studying the quenching of jets by the quark-gluon plasma, we aim to discover more about not only these jets themselves, but also about the quark-gluon plasma.

In figure 1 we see one of the experimental indications of the existence of jet quenching. In this figure the ratio between the amount of jets at a certain p_T in Pb-Pb collisions and the amount of jets expected at that p_T from similar p-p collisions, this is defined as a measure of how quenched a jet is and called R_{AA}. We expect quenching effects to be largest for particles that collide head-on, this is confirmed by the fact that the graph for 0-10% centrality shows the lowest R_{AA} and is most suppressed by jet quenching.
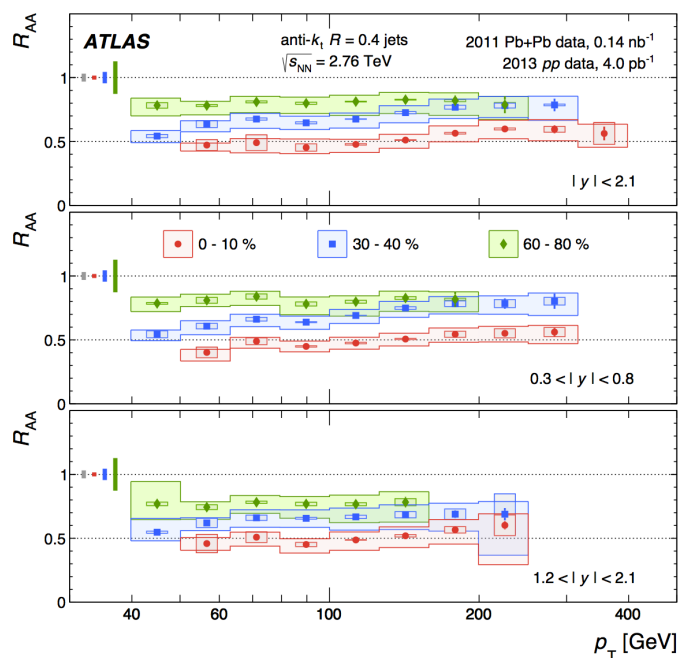

Figure 1: The R_{AA} as a function of the jet p_T for different centralities.(Image: ATLAS Experiment/CERN)[13]

The two largest contributers to the energy loss of the partons is through collisional energy loss and radiative energy loss. At low parton momentum elastic scatterings make up the main part of the energy loss, also called collisional energy loss. At higher momenta this is through inelastic scattering, or radiative energy loss. Though other energy loss effects are present, in most cases they are far less significant.[14]

2.3   Monte Carlo Simulation

Monte Carlo simulations are the primary way to study particle collisions, apart from the experiments done in particle accelerators, such as the LHC and RHIC. The PYTHIA 8 software, created by Lund University, is used to simulate baseline unquenched p-p events, while JEWEL software can simulate the quenched Au-Au and Pb-Pb collisions. To create the PYTHIA events, we used the JetToyHI software[15], which is build upon the PYTHIA software.

The PYTHIA software works by first simulating a small amount of partons per event, as well as the nature of the first event. This gives a very broad structure to the event. From this initial event all activity and interaction of the partons is calculated. From the final partons, hadronization is calculated, including the decay of unstable hadrons.[16] In essence the JEWEL software works similarly, but is modified to simulate jet quenching.

When comparing simulated jets to experimental results, we see that the JEWEL settings we used systematically underestimate the jet mass. This is due to the fact that we do not take recoils into account. This means that we do not account for partons that scatter out of the medium. While the software can simulate these scatterings, the resulting overestimation of the mass gives less accurate results for the current version.[17][18] However, these comparisons have not been done for Au-Au collisions, nor for the low p_T range for which we will do the comparisons. But similar results are to be expected.
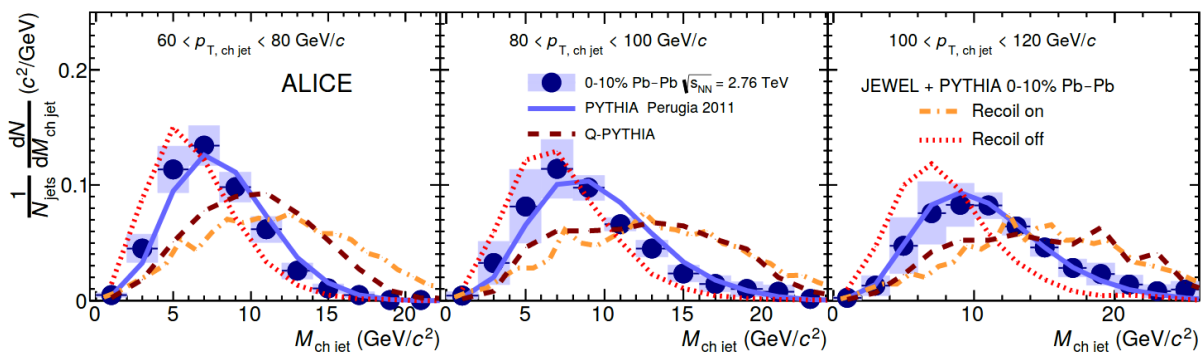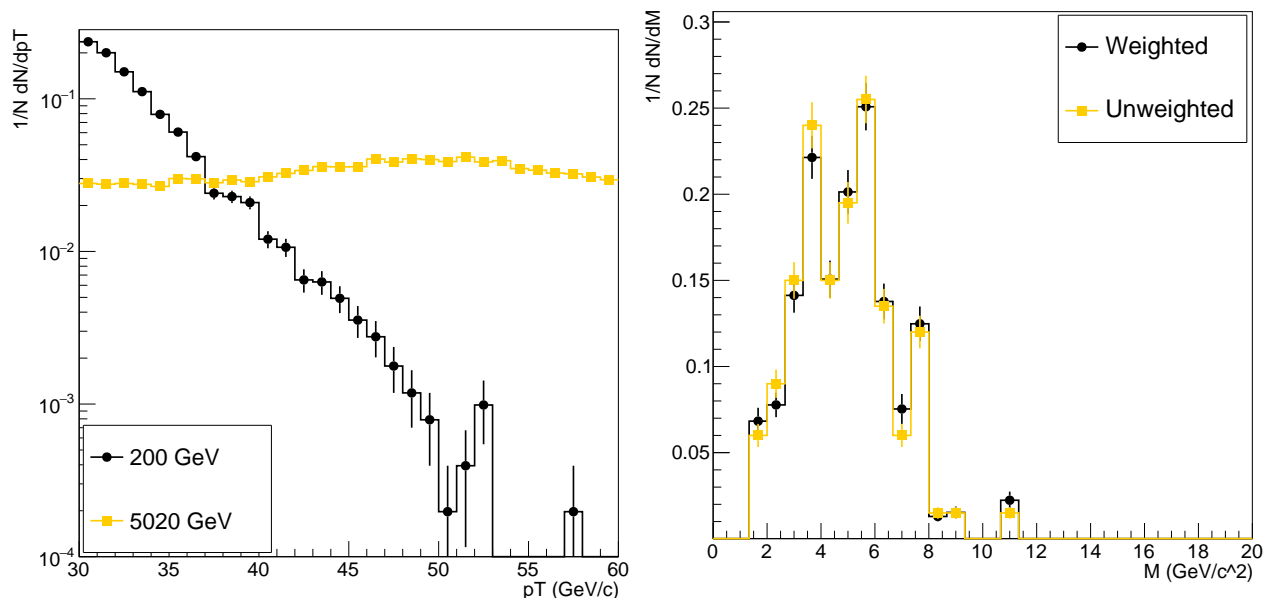

Figure 2: Jet mass distribution for PYTHIA and JEWEL simulations with and without recoils, as well as experimental data. (Image: ALICE collaboration/CERN)[17]

This is illustrated in figure 2 where we see that the average jet mass for JEWEL with recoils on is higher than the experimental data. While slightly lower, the average jet mass for JEWEL with recoils off conforms better to the experimental data.

3   Simulation Method

We will be using simulations to study the quenching effects for Au-Au collisions at 200 GeV, as well as Pb-Pb collisions at 5020 GeV. PYTHIA was used to generate two sets of p-p events. One with an energy of 200 GeV, the other at 5020 GeV. These datasets are used as a unquenched baseline. We compare this baseline with two quenched datasets, one Au-Au at 200 GeV and one Pb-Pb at 5020 GeV, generated by JEWEL. From these datasets we will be selecting for a p_T between 30 GeV/c and 60 GeV/c. At 200 GeV jets above 60 GeV/c are rare, so to get a p_T range at which we have jets for both the simulation run at 200 GeV as well as the simulation at 5020 GeV we used an upper boundary of 60 GeV/c. The lower boundary of 30 GeV/c is due to the fact that below 30 GeV/c jets are not well defined. After this selection, we will be looking at the jet mass, jet width, $p_T D$ and the Soft Drop groomed jet mass. All events generated are of head-on collisions, with a centrality of 0-5 %. The Monash 2013 tune by Peter Skands is used for the PYTHIA simulations.[19]

Looking at a p_T between 30 GeV/c and 60 GeV/c in figure 3a, for 5020 GeV we have a relatively even distribution of p_T, but at 200 GeV the distribution drops for higher p_T. To eliminate the effects of the p_T on the other observables, weights are given to the observables for the 200 GeV simulations equal to the p_T of the 5020 GeV simulation divided by the 200 GeV simulation. The amount of events we generated are in the order of $10^4 - 10^5$. More events were needed for the 200 GeV simulations, as the amount of jets with a p_T between 50 and 60 GeV/c approached zero. In figure 3a we see that some bins are still zero, as the amount of events was still too low.

(a) PYTHIA simulation p_T distribution, for 5020 and 200 GeV.

(b) The jet mass distributino for quenched JEWEL simulation for Au-Au collisions at 200 GeV.

Figure 3

To counteract this, wider bins were used to calculate the weights. Though this gives less accurate weights, it does give workable results. The weights used can be seen in figure 4 for both the PYTHIA and JEWEL simulation. Using these weights results in a slight shift, as illustrated in figure 3b. To get results in the common p_T-range between 30 GeV/c and 60 GeV/c, a minimum invariant transverse momentum $\hat{p_T} = 20$ was used for the 5020 GeV simulations and $\hat{p_T} = 10$ for the 200 GeV simulations. This $\hat{p_T}$ is related to the energy transfer of the initial hard parton reaction. This $\hat{p_T}$ needs to be lower than the lowest p_T used, so lower than 30 GeV/c. The histograms were normalized to total integral of unity, as we are interested in the means and shape of the histograms.
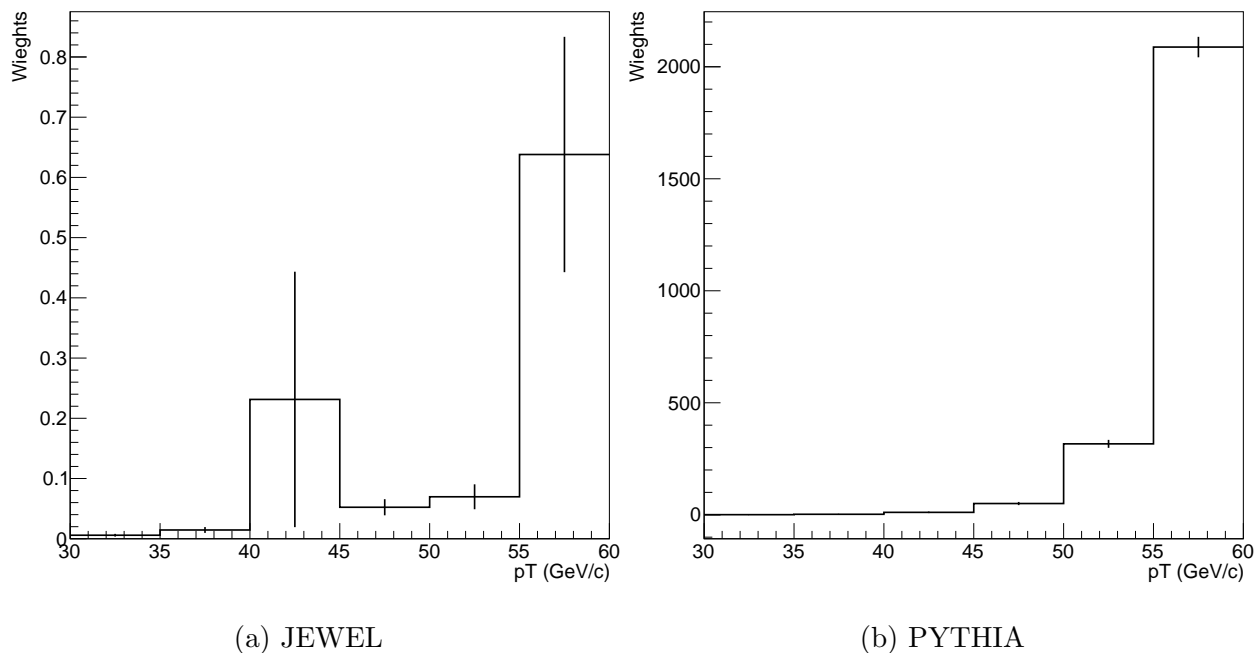

(a) JEWEL   (b) PYTHIA

Figure 4: The weights used, calculated by dividing the p_T at 5020 GeV by the p_T at 200 GeV for the JEWEL and PYTHIA simulation.

4   Results

For the different observables we study the mean and standard deviation of the results of the simulation. Comparing these values for the PYTHIA (unquenched) and JEWEL (quenched) simulations will tell us for which observables and at which energies the effects of jet quenching will best be observed. We will first take a look at the jet mass distributions, which we will later compare to the jet mass of the jet, groomed by the Soft Drop algorithm. This comparison eliminates hadronization as the primary contributer to any differences between the JEWEL and PYTHIA simulations. This leaves interaction between the partons and the quark-gluon plasma as the main contributer. After this, we will look at the jet width, to eliminate the statistical error of the jet mass calculation due to not taking into account recoils, as the main contributer to any differences in means and standard deviations between the quenched and unquenched simulations.

4.1 Jet Mass
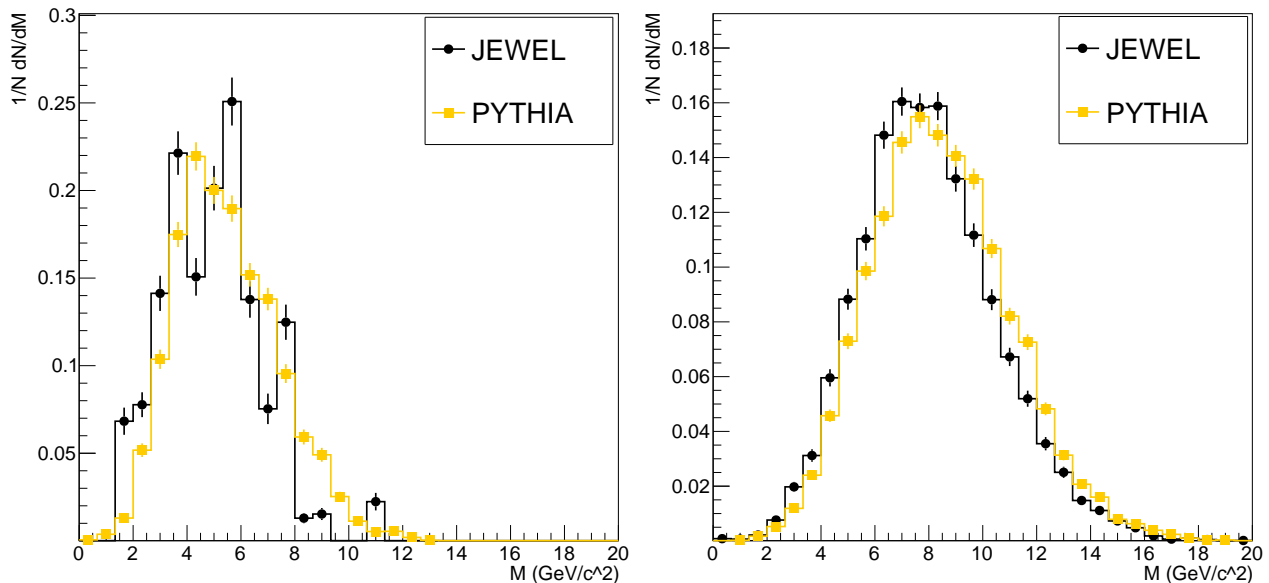
(a) 200 GeV p-p PYTHIA simulation.
200 GeV Au-Au JEWEL simulation.

(b) 5020 GeV p-p PYTHIA simulation.
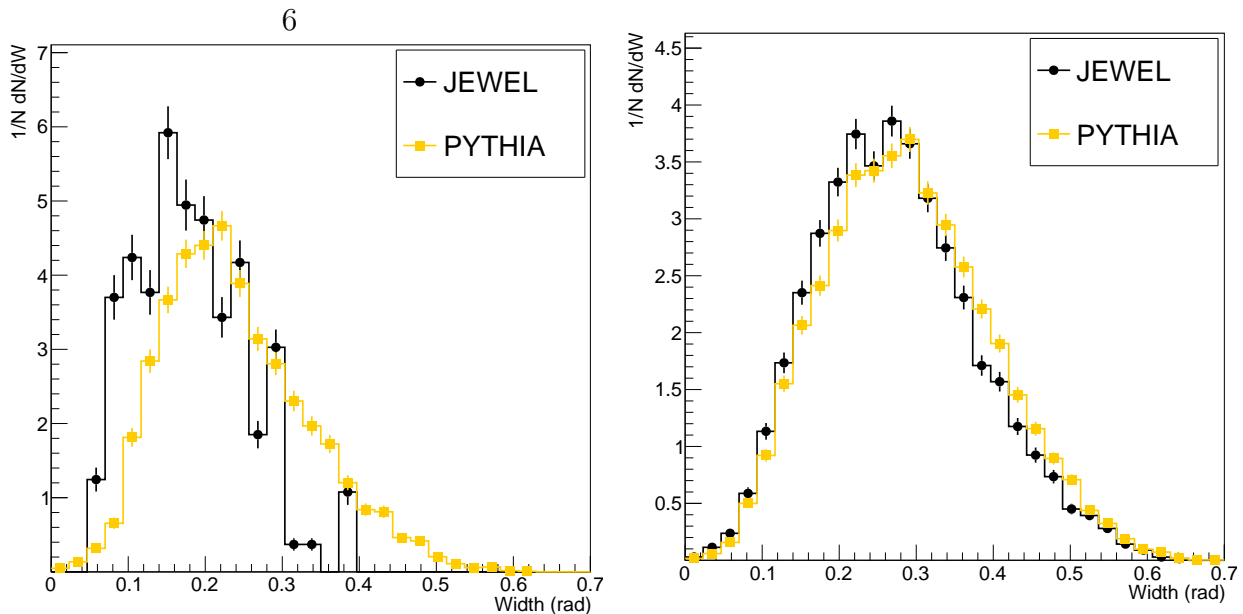5020 GeV Pb-Pb JEWEL simulation.

Figure 5: Jet mass distribution for JEWEL and PYTHIA simulations.

Studying the jet mass distributions we observe a drop in average mass at both 200 GeV and 5020 GeV, as illustrated in figure 5. At 200 GeV we observe the largest drop both absolutely and relatively, in table 1 we see that the average has decreased 0.514 ± 0.0687 GeV/c^2 for the quenched results, which is a relative decrease of $9.4 \pm 1.3\%$. This in comparison to the average jet mass at 5020 GeV, which dropped 0.458 ± 0.0494 GeV/c^2 for the quenched results, a relative decrease of $5.4 \pm 0.6\%$. This physical interpretation of this decrease is that less hadrons are included in the definition of the jet and the hadrons left in the jet are more collimated. These hadrons can still be created, the jet algorithm does not include them in the jet however. How much of this decrease can be attributed to the anticipated decrease due to not taking into account recoils when simulating these results, is unclear. The standard deviation also decreases a small amount for the quenched results at 200 GeV, but with an error estimation in the order of the difference itself, this is not significant. The decrease in standard deviation for the simulations at 5020 GeV is significant however, showing a decrease of $2.2 \pm 1.4\%$.

200 GeV	mean	std dev	5020 GeV	mean	std dev
JEWEL	4.973 ± 0.0417	1.839 ± 0.0295	JEWEL	8.017 ± 0.0267	2.546 ± 0.0189
PYTHIA	5.487 ± 0.0270	1.916 ± 0.0191	PYTHIA	8.475 ± 0.0227	2.602 ± 0.0160
Difference	0.514 ± 0.0687	0.0077 ± 0.0486	Difference	0.458 ± 0.0494	0.056 ± 0.0349

Table 1: Means and standard deviations in GeV/c^2 of the jet mass distributions, at 200 GeV and 5020 GeV for both PYTHIA and JEWEL, shown in figure 5.

4.2   Jet Width

(a) 200 GeV p-p PYTHIA simulation.
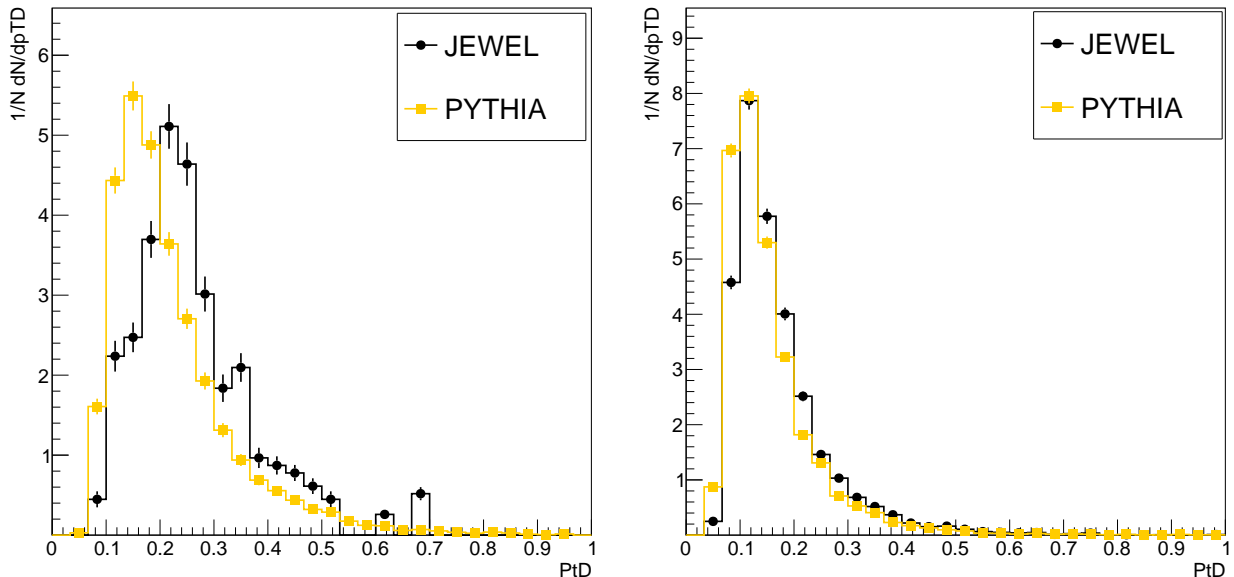200 GeV Au-Au JEWEL simulation.

(b) 5020 GeV p-p PYTHIA simulation.
5020 GeV Pb-Pb JEWEL simulation.

Figure 6: Jet width distribution for JEWEL and PYTHIA simulations.

Similar to the differences in the jet mass distributions, in figure 6 we observe a drop in average jet width at both 200 GeV and 5020 GeV. At 200 GeV the average jet width is $5.74\pm0.294\times10^{-2}$ radians lower for the quenched simulation as shown in table 2, a $24.0\pm1.4\%$ decrease. At 5020 GeV the quenched simulation is still decreased, but less so. We observe a decrease of $1.46 \pm 0.205 \times 10^{-2}$ radians for the quenched results, a relative decrease of $5.1 \pm 0.8\%$. The standard deviation shows a decrease as well, with the standard deviation for the 200 GeV distribution being $23.0 \pm 2.5\%$ smaller for the quenched result, whereas the standard deviation for the 5020 GeV simulations showed a decrease of $2.4 \pm 1.4\%$.

200 GeV	mean	std. dev.	5020 GeV	mean	std. dev.
JEWEL	1.826 ± 0.016	0.7347 ± 0.0117	JEWEL	2.753 ± 0.0111	1.056 ± 0.0079
PYTHIA	2.4 ± 0.0134	0.9538 ± 0.0095	PYTHIA	2.899 ± 0.0094	1.081 ± 0.0067
Difference	0.574 ± 0.0294	0.2191 ± 0.0212	Difference	0.146 ± 0.0205	0.025 ± 0.0146

Table 2: Means and standard deviations in 10^{-1} radians of the jet width distributions, at 200 GeV and 5020 GeV for both PYTHIA and JEWEL, shown in figure 6.

4.3   Jet $p_T D$

(a) 200 GeV p-p PYTHIA simulation.
200 GeV Au-Au JEWEL simulation.

(b) 5020 GeV p-p PYTHIA simulation.
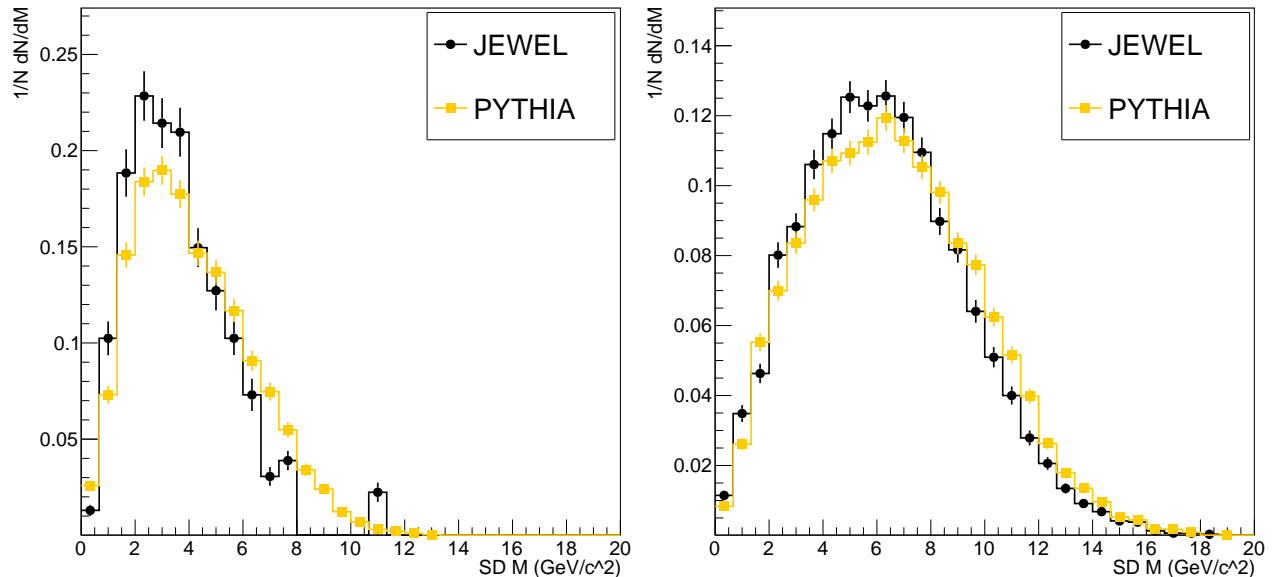5020 GeV Pb-Pb JEWEL simulation.

Figure 7: Jet $p_T D$ distribution for JEWEL and PYTHIA simulations.

The $p_T D$ shows an increase for the quenched simulation over the unquenched simulation, as can be seen in figure 7. In table 3 we see that at 200 GeV the $p_T D$ increases by $4.32 \pm 0.4444 \times 10^{-2}$ for the quenched results, a relative increase of $19.6 \pm 2.2\%$. At 5020 GeV it increases by $1.77 \pm 0.178 \times 10^{-2}$, a relative increase of $11.5 \pm 1.2\%$. At 200 GeV the standard deviation showed no significant change, but at 5020 GeV the standard deviation showed an increase of $9.5 \pm 1.5\%$. These increases indicate quenched simulations to be more quark-like for both the 200 GeV and the 5020 GeV simulations, their unquenched counterparts appear more gluon-like.

200 GeV	mean	std dev	5020 GeV	mean	std dev
JEWEL	2.636 ± 0.0260	1.148 ± 0.0184	JEWEL	1.716 ± 0.0100	0.972 ± 0.0070
PYTHIA	2.204 ± 0.0184	1.168 ± 0.0116	PYTHIA	1.539 ± 0.0078	0.8886 ± 0.0055
Difference	0.432 ± 0.0444	0.02 ± 0.03	Difference	0.177 ± 0.0178	0.0834 ± 0.0125

Table 3: Means and standard deviations in 10^{-1} dimensionless units of the jet $p_T D$ distributions, at 200 GeV and 5020 GeV for both PYTHIA and JEWEL, shown in figure 7.

4.4   Soft Drop Jet Mass

(a) 200 GeV p-p PYTHIA simulation.
200 GeV Au-Au JEWEL simulation.

(b) 5020 GeV p-p PYTHIA simulation.
5020 GeV Pb-Pb JEWEL simulation.

Figure 8: Soft Drop jet mass distribution for JEWEL and PYTHIA simulations.

After grooming the jets with the Soft Drop algorithm, we find similar results for the jet mass as for the ungroomed jets in figure 8. The Soft Drop jet mass less sensitive to hadronization effects, in contrast to the jet mass, which has a strong hadronization dependence. By comparing the jet mass to the Soft Drop jet mass, we can confirm that the shift in average jet mass is due to the interactions between the partons and the medium, the quark-gluon plasma. From the differences in table 4 we calculate the relative differences. At 200 GeV quenching leads to a $12.1 \pm 1.9\%$ decrease in jet mass in our simulation. At 5020 GeV this decrease is $5.2 \pm 1.0\%$. These relative differences are quite similar to the differences found for the jet mass, excluding hadronization effects as the main contributer to the shift in jet mass. The standard deviation at 200 GeV is $12.9 \pm 2.5\%$ lower for the quenched jets, while at 5020 GeV it is $4.8 \pm 1.4\%$ lower.

200 GeV	mean	std dev	5020 GeV	mean	std dev
JEWEL	3.672 ± 0.0440	1.939 ± 0.0311	JEWEL	6.312 ± 0.0319	3.035 ± 0.0225
PYTHIA	4.175 ± 0.0314	2.225 ± 0.0222	PYTHIA	6.659 ± 0.0278	3.185 ± 0.0196
Difference	0.503 ± 0.0754	0.286 ± 0.0533	Difference	0.347 ± 0.0597	0.15 ± 0.0421

Table 4: Means and standard deviations in GeV/c^2 of the Soft Drop jet mass distributions, at 200 GeV and 5020 GeV for both PYTHIA and JEWEL, shown in figure 8.

5   Conclusion

Comparing the unquenched jet masses to the quenched jet masses, we find a significant drop in average jet mass for the quenched jets at both 200 GeV and 5020 GeV, the drop at 200 GeV being larger. It is unclear however, if this drop is due to the simulation not taking into account recoils, hadronization effects or parton-medium interactions. While the jet width is still dependent on the angle, just as the jet mass is, is more dependent on the momentum than the jet mass is. So while a statistical lowering due to not accounting for recoils is still expected, this has less impact on the jet width, than it has on the jet mass. As the average jet width has a larger drop for quenched jets, than the jet mass has, quenching effects seem to have a larger contribution to this shift. Furthermore, as we see a similar shift in the average jet mass for both the Soft Drop groomed results, as well as the ungroomed results, we can also exclude hadronization effects as the main contributer to the shift.

For both 200 GeV and 5020 GeV quenched jets have a higher average $p_T D$ than unquenched jets. This points to the quenched jets containing relatively more quarks than unquenched jets and comparing the $p_T D$ can thus be a viable way to determine if a jet is quenched or not.

All observed shifts are larger at 200 GeV than 5020 GeV, both absolute and relative. While the observables of the quenched and unquenched jets have consistently different averages, quenching effects are larger at low energies. When studying quenching effects it can be useful to consider studying lower energy collisions, as quenching effects will then be easier to detect. A general recommendation can be made for research of quenching effects to study the jet width at lower energies, comparing Au-Au collisions to p-p collisions at similar energies.

6   Discussion

While a large sample size was used to try to get enough jets at 200 GeV with a p_T between 30 GeV/c and 60 GeV/c, this was not fully succesful, as can be seen in figure 9. For better results a sample size of in the order of 10^7 events or more is needed. Instead of using the bin values of figure 3a as weights to eliminate the influence the p_T has on other observables, these graphs can be fitted for more accurate results. This also takes into account the large errorvalue the weight has for 40 GeV/c $< p_T <$ 45 GeV/c, where taking the binvalue does not. Taking the fit instead of the binvalues also diminishes the deficit of statistics in the 55 GeV/c $< p_T <$ 60 GeV/c range.

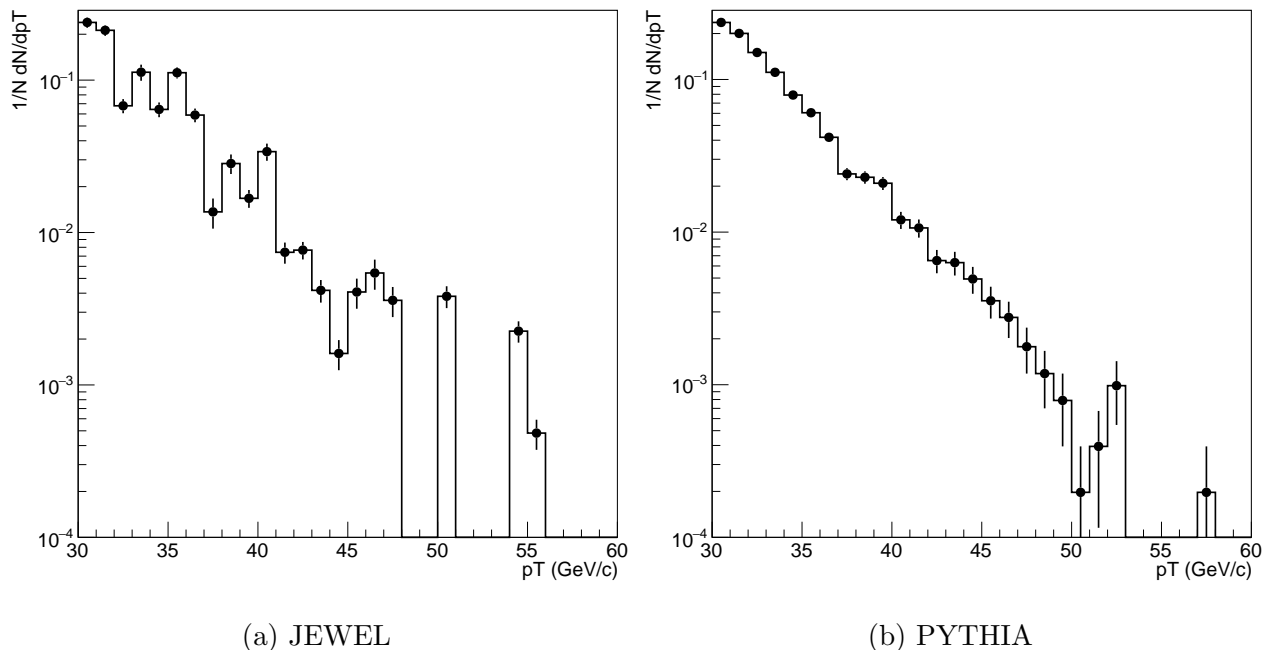(a) JEWEL   (b) PYTHIA

Figure 9

Because of the underestimation of the jet mass by the JEWEL software, when not taking into account recoils, a similar study to the one in this thesis is needed which does take into account recoils for a more definite conclusion on the quenching effects on the jet mass. Comparisons to experimental data can be done in addition as well.

Additional research can be done to account for the difference in ratio of quarks and gluon between the 200 GeV and 5020 GeV jets. The 5020 GeV jets contain more gluons than quarks, while the 200 GeV jets contain approximately equal amounts of gluons and quarks. Because of this, differences in quenching effects on quarks and gluons must be taken into account.

References

[1] Z22, *A section of relativistic heavy ion collider (rhic) at brookhaven national laboratory (bnl) in united states* (2017), used under the Creative Commons Attribution-Share Alike 4.0 International license. https://creativecommons.org/licenses/by-sa/4.0/legalcode.

[2] T. Ludlam, Physics Today (2003), URL `https://physicstoday.scitation.org/doi/10.1063/1.1629004`.

[3] S. Ozaki (2001), vol. 1, pp. 1 – 5 vol.1, ISBN 0-7803-7191-7.

[4] J. Casalderrey-Solana and C. A. Salgado, *Introductory lectures on jet quenching in heavy ion collisions* (2007), `0712.3443`.

[5] *Cern: The large hadron collider*, URL `https://home.cern/science/accelerators/large-hadron-collider`.

[6] S. Marzani, G. Soyez, and M. Spannowsky, Lecture Notes in Physics (2019), ISSN 1616-6361, URL `http://dx.doi.org/10.1007/978-3-030-15709-8`.

[7] M. Cacciari, G. P. Salam, and G. Soyez, The European Physical Journal C **72** (2012), ISSN 1434-6052, URL `http://dx.doi.org/10.1140/epjc/s10052-012-1896-2`.

[8] G. Aad, B. Abbott, J. Abdallah, S. Abdel Khalek, A. A. Abdelalim, O. Abdinov, B. Abi, M. Abolins, O. S. AbouZeid, H. Abramowicz, et al., Physical Review D **86** (2012), ISSN 1550-2368, URL `http://dx.doi.org/10.1103/PhysRevD.86.072006`.

[9] Tech. Rep. CMS-PAS-JME-16-003, CERN, Geneva (2017), URL `https://cds.cern.ch/record/2256875`.

[10] M. Dasgupta, A. Fregoso, S. Marzani, and G. P. Salam, Journal of High Energy Physics **2013** (2013), ISSN 1029-8479, URL `http://dx.doi.org/10.1007/JHEP09(2013)029`.

[11] A. J. Larkoski, S. Marzani, G. Soyez, and J. Thaler, Journal of High Energy Physics **2014** (2014), ISSN 1029-8479, URL `http://dx.doi.org/10.1007/JHEP05(2014)146`.

[12] J. Casalderrey-Solana, G. Milhano, D. Pablos, and K. Rajagopal, Journal of High Energy Physics **2020** (2020), ISSN 1029-8479, URL `http://dx.doi.org/10.1007/JHEP01(2020)044`.

[13] G. Aad, B. Abbott, J. Abdallah, S. Abdel Khalek, O. Abdinov, R. Aben, B. Abi, M. Abolins, O. AbouZeid, H. Abramowicz, et al., Physical Review Letters **114** (2015), ISSN 1079-7114, URL `http://dx.doi.org/10.1103/PhysRevLett.114.072302`.

[14] D. d'Enterria and B. Betz, *High-pT Hadron Suppression and Jet Quenching* (2009), vol. 785, pp. 285–339.

[15] M. Verweij, `https://github.com/mverwe/JetToyHI/tree/forbsc` (2020), gitHub repository: JetToyHI.

[16] S. M. Torbjörn Sjöstrand and P. Skands, Elsevier (2007), URL https://doi.org/10.1016/j.cpc.2008.01.036.

[17] S. Acharya, D. Adamov, M. Aggarwal, G. Aglieri Rinella, M. Agnello, N. Agrawal, Z. Ahammed, N. Ahmad, S. Ahn, S. Aiola, et al., Physics Letters B **776**, 249264 (2018), ISSN 0370-2693, URL http://dx.doi.org/10.1016/j.physletb.2017.11.044.

[18] R. Kunnawalkam Elayavalli and K. C. Zapp, Journal of High Energy Physics **2017** (2017), ISSN 1029-8479, URL http://dx.doi.org/10.1007/JHEP07(2017)141.

[19] P. Skands, S. Carrazza, and J. Rojo, The European Physical Journal C **74** (2014), ISSN 1434-6052, URL http://dx.doi.org/10.1140/epjc/s10052-014-3024-y.